Risø–R–1354(EN)

A Beddoes-Leishman type dynamic stall model in state-space and indicial formulations

Morten Hartvig Hansen
Mac Gaunaa
Helge Aagaard Madsen

Risø National Laboratory, Roskilde, Denmark
June 2004

Abstract This report contains a description of a Beddoes-Leishman type dynamic stall model in both a state-space and an indicial function formulation. The model predicts the unsteady aerodynamic forces and moment on an airfoil section undergoing arbitrary motion in heave, lead-lag, and pitch. The model includes the effects of shed vorticity from the trailing edge (Theodorsen Theory), and the effects of an instationary trailing edge separation point. The governing equations of the model are nonlinear, and they are linearized about a steady state for application in stability analyzes. A validation is carried out by comparing the response of the model with inviscid solutions and observing the general behavior of the model using known airfoil data as input. The proposed dynamic model gives results identical to inviscid solutions within the attached-flow region; and it exhibits the expected dynamic features, such as overshoot of the lift, in the stall region. The linearized model is shown to give identical results to the full model for small amplitude oscillations. Furthermore, it is shown that the response of finite thickness airfoils can be reproduced to a high accuracy by the use of specific inviscid response functions.

ISBN 87-550-3089-0; 87-550-3090-4 (Internet)
ISSN 0106–2840

Contents

Notations

a^{st}	Arm to equivalent pressure center
A_1, A_2	Constants in the approximation to the indicial function ϕ
b_1, b_2	Exponents in the approximation to the indicial function ϕ
A_x	Amplitude of lead-lag motion of the airfoil
c	Chord length
C_L	Lift coefficient
$C_{L,\alpha}$	Linear lift slope coefficient
C_D	Drag coefficient
C_M	Moment coefficient
f	Non-dimensional position of the separation point
$h_{1/2}$	Heave coordinate at mid-chord
k	Reduced frequency $\omega c/(2U_0)$.
P_i, Q_i	Terms in linear first order equations
s	Non-dimensional time $\frac{2}{c}\int_0^t U dt$
t	Time
T_0	Characteristic time equal the to travel-time of one half chord $c/(2U_0)$
T_1	Time lag related to the shed wake effect T_0/b_1
T_2	Time lag related to the shed wake effect T_0/b_2
T_f	Characteristic time lag related to the pressure distribution
T_u	Time-varying time constant $c/(2U(t))$
T_p	Characteristic time lag related to the separation point
U	Relative velocity of the air dependent of airfoil motion
U_0	Free stream velocity
$w_{3/4}$	Downwash at three-quarter chord point
x_i	Aerodynamic state variables
y_1, y_2	Aerodynamic state variables related to the downwash $w_{3/4}$
α	Angle of attack
$\alpha_{3/4}$	Angle of attack at three-quarter chord point
ω	Angular velocity
λ	Relative magnitude of stream-wise velocity amplitude $\omega A_x/U_0$
ρ	Density of air
ϕ	Indicial function for lift response

1 Introduction

A new Beddoes-Leishman (B-L) type model of unsteady airfoil aerodynamics and dynamic stall is suggested. Both state-space and indicial formulations of the model are presented. The explicit state-space formulation enables stability analysis for wind turbines based on eigenvalue analysis, and the implicit indicial formulation is presented for effective numerical solution of the aeroelastic equations. An indicial version of the original B-L model has already for some time been used in the aeroelastic code HAWC [1, 2].

An unsteady aerodynamic model is used to describe the unsteady aerodynamic forces on an airfoil undergoing arbitrary motion in a flow. Since the first aeroelastic calculations on aircrafts began, unsteady airfoil aerodynamics has been studied experimentally and theoretically. Theodorsen's potential flow approximation to the unsteady lift and pitching moment [3] formed the basis for analysis of fixed wing aircrafts operating below stall in the attached flow region. The occurrence of stall flutter of propellers, compressors, and rotor wings, and the continuous optimization of helicopter design led to the need for analysis of unsteady aerodynamic forces in the stalled region. Until the 50's the phenomenon *dynamic stall* was only studied experimentally (see e.g. [4]); the first analytical dynamic stall models were introduced in the late 70's. Friedmann describes three models in his review paper from 1983 [5]; since then models have improved and others have been introduced.

Very few of these models are originally formulated in the state-space, one example is the ONERA model [6, 7]. The B-L model was originally introduced in a form using indicial functions because this is computationally the most effective formulation. There are many publications on the model; early papers by Beddoes [8, 9, 10] deals with the unsteady lift and pitching moment. These papers are followed by a cooperative paper by Leishman and Beddoes [11] introducing a complete model for unsteady lift, drag, and moment. A revised version of this work is given in [12]. The B-L model includes the effect of the unsteady two-dimensional inviscid wake, the effects of trailing and leading edge flow separation, and compressibility effects similar to the Piston Theory. State-space formulations of the B-L model have been published for attached flow conditions in [13, 14] and for the complete dynamic stall model in [15]. Details on the computation of unsteady drag is given by Leishman in [16], and an extension of the modelling of the near wake is given by Beddoes in [17] taking into account spanwise effects. A general review of unsteady airfoil aerodynamics can be found in [18].

This report introduces new state-space and indicial formulations of a dynamic stall model very similar to the B-L model. The suggested model is intended for wind turbine aeroelasticity, where compressibility effects and flow separation initiated from the leading edge can be neglected. This is due to a typical maximum tip speed of 70–80 m/s and the use of relative thick airfoils with a typical thickness of no less than 15 %. Hence, the B-L model is modified to assume incompressibility and the unsteady effects of leading edge flow separation is removed. Wind turbines have the risk of stall-induced lead-lag vibrations. The unsteady lift due to the time-varying flow velocity for an airfoil vibrating in lead-lag [19] is therefore included in the present state-space formulation, which is not the case in previous state-space formulations of the B-L model [13, 14]. For the implementation of the present model in aeroelastic wind turbine codes, an indicial formulation is provided and the robustness of the model with respect to the input has been kept in mind. The only input is the static lift, drag, and moment curves, four constants determining the unsteady inviscid response (two time-constants), and two time-constants determining the unsteady viscous effects.

The report is arranged as follows: In Section 2 the suggested B-L type dynamic

stall model is described by its state-space formulation, including a linearization of the model. An indicial formulation of the model is described in Section 3, and in Section 4 the suggested empirical model is compared to numerical solutions of Euler and Navier-Stokes equations.

2 State-space formulation

The state-space formulation of the suggested dynamic stall model is presented in this section. The dynamics of the aerodynamic system is related to the lift, and the unsteady drag and pitching moment are then determined from the unsteady lift. The section is therefore divided into three subsections describing these three forces separately, followed by a subsection presenting the closed set of nonlinear equations, and finally a subsection dealing with the linearization of the model.

2.1 Lift

The original B-L model includes leading edge separation and the impulsive forces due to compressibility. For wind turbines, Mach numbers are lower than 0.3 and it is assumed that the flow is incompressible, whereby added mass forces substitute the impulsive forces. Furthermore, the leading edge (LE) separation is assumed not to be a dominating phenomenon for the relative thick airfoils used on wind turbine blades. These assumptions lead to an alternative formulation of the model where lift under attached flow conditions is given by the Theodorsen Theory, and only trailing edge (TE) separation is considered under stalled flow conditions.

Attached flow

The unsteady lift on a symmetric airfoil performing harmonic pitch and plunge motion of small amplitude in an attached flow can be approximated by the Theodorsen Theory [3]. The unsteady effect of vortex shedding due to changes in circulation on the airfoil is derived analytically by assuming that the airfoil is infinitely thin, and that the vortex wake is harmonic and travels with the free-stream velocity in a straight line behind the airfoil, as shown schematically in Figure 1.

The downwash at the three-quarter point $w_{3/4}$ depends only on the pitch and plunge motion of the airfoil, and the free-stream velocity U is assumed to be constant in Theodorsen's original derivations. A time-varying free-stream velocity from air turbulence and arbitrary motion of the airfoil (e.g. combination of plunge and lead-lag) are not included because the pure harmonic wake assumption fails in these cases. Different approximations to the Theodorsen Theory have been developed to handle these cases; a study of these approximate theories can be found in [19].

Van der Wall and Leishman concluded that for moderate reduced frequencies, all theories give the same result as the Theodorsen theory, when a time-varying free-stream velocity $U = U(t)$ is inserted in the Duhamel's integral formulation. In this case, the unsteady lift is given as

$$L = \pi\rho\frac{c^2}{4}\left(U\dot{\alpha} + \dot{U}\alpha + \ddot{h}_{1/2}\right) + \pi\rho cU\left(w_{3/4}(0)\,\phi(s) + \int_0^s \frac{dw_{3/4}}{d\sigma}\,\phi(s-\sigma)\,d\sigma\right) \quad (1)$$

where $(\dot{}) \equiv \partial/\partial t$, c is the chord length, ρ is the air density, α is the geometric angle of attack between chord and free-stream flow, $\ddot{h}_{1/2}$ is the plunge acceleration

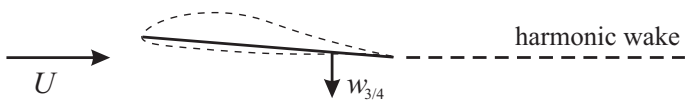

Figure 1. Schematic of the assumptions of the Theodorsen theory.

at the mid-chord, ϕ is an *indicial function*, and s is the non-dimensional time-scale

$$s = \frac{2}{c}\int_0^t U dt \tag{2}$$

describing the distance travelled by the wake in the time-varying free-stream.

The first term in (1) is the non-circulatory part of the lift due to acceleration of the air mass $\pi\rho c^2/4$. For moderate reduced frequencies, the acceleration parts of this term $\ddot{h}_{1/2}$ and $\dot{U}\alpha$ will be an order lower than the velocity part $U\dot{\alpha}$, and these terms are therefore neglected in the modelling of the added mass term.

The second term in (1) is the circulatory lift with Duhamel's integral describing the memory effect of previously shed vorticity into the wake. The integral (2) can not be evaluated analytically, because the free-stream velocity U is a nonlinear function of the structural state variables describing the arbitrary airfoil motion. However, it is still possible to replace the memory term in (1) with a set of state-space differential equations that are nonlinear in the state variables. The memory term can be considered as an effective downwash at the three-quarter point

$$w_{3/4}^{\text{eff}} = w_{3/4}(0)\,\phi(s) + \int_0^s \frac{dw_{3/4}}{d\sigma}\,\phi(s-\sigma)\,d\sigma \tag{3}$$

By integration by parts on Duhamel's integral yields

$$w_{3/4}^{\text{eff}} = w_{3/4}(s)\,\phi(0) - \int_0^s w_{3/4}(\sigma)\,\frac{d\phi}{d\sigma}(s-\sigma)\,d\sigma \tag{4}$$

Performing the variable substitution (2) for σ and s, the effective downwash can be written as

$$w_{3/4}^{\text{eff}} = w_{3/4}(t)\,\phi(0) - \int_0^t w_{3/4}(t')\,\frac{d\phi}{dt'}\left(\frac{2}{c}\int_{t'}^t U(\tau)d\tau\right)\,dt' \tag{5}$$

where t and t' are related to s and σ, respectively, through (2).

For a step-change in angle of attack the indicial function ϕ is the Wagner function, and for sharp edge gust it is the Küssner function. Both functions are often approximated by two time-lags as

$$\phi(s) = 1 - A_1 e^{-b_1 s} - A_2 e^{-b_2 s} \tag{6}$$

where the constants A_1, A_2, b_1, and b_2 may vary depending on application (see e.g. [10] for values for helicopter applications).

The two time-lags terms of ϕ can be represented by two first order differential equations. Substitution of (6) with $s = \frac{2}{c}\int_{t'}^t U(\tau)d\tau$ into (5), and differentiation with respect to t' yields

$$\frac{d\phi}{dt'}\left(\frac{2}{c}\int_{t'}^t U(\tau)d\tau\right) = -\frac{2U(t')}{c}\sum_{i=1}^2 b_i A_i e^{-b_i\frac{2}{c}\int_{t'}^t U(\tau)d\tau} \tag{7}$$

Substitution of (7) into (5) yields that the effective downwash can be written as

$$w_{3/4}^{\text{eff}} = w_{3/4}(t)(1 - A_1 - A_2) + y_1(t) + y_2(t) \tag{8}$$

where the new state variables y_i are

$$y_i(t) = b_i A_i \frac{2}{c}\int_0^t w_{3/4}(t')\,U(t')e^{-b_i\frac{2}{c}\int_{t'}^t U(\tau)d\tau}\,dt' \tag{9}$$

where $i = 1, 2$. Differentiation (9) with respect to t shows that aerodynamic state y_i is the solution to the differential equation

$$\dot{y}_i + b_i\frac{2U}{c}\,y_i = b_i A_i \frac{2U}{c}\,w_{3/4} \tag{10}$$

where $i = 1, 2$ and $y_i(0) = 0$. The equation is linear in the aerodynamic state variable y_i, however these states couple nonlinearily to the structural states through the dependency of U.

Hence, the ODEs (10) for the effective downwash determine the dynamics of the near wake influence on the unsteady lift coefficient for attached flow. However, this formulation in downwash $w_{3/4}$ is inconvenient because the definition of downwash is ambiguous in the large range of angles of attack that a wind turbine blade encounters. The original B-L formulation in geometrical angle of attack at the three-quarter point $\alpha_{3/4}$ is therefore applied.

Using the relation $\alpha_{3/4} = w_{3/4}/U$ and introducing the variable transformation $y_i = Ux_i$, the ODEs (10) become

$$\dot{x}_i + \frac{2U}{c}\left(b_i + \frac{c\,\dot{U}}{2\,U^2}\right) x_i = b_i A_i \frac{2U}{c}\,\alpha_{3/4} \tag{11}$$

with initial conditions $x_i(0) = 0$, and where it has been assumed that the free-stream velocity U is non-zero. With the new state variables x_1 and x_2, it is possible to compute an effective angle of attack

$$\alpha_E = \alpha_{3/4}(1 - A_1 - A_2) + x_1(t) + x_2(t) \tag{12}$$

whereby the unsteady lift for attached flow (1) can be rewritten as

$$C_L^p = 2\pi(\alpha_E - \alpha_0) + \pi c\,\dot{\alpha}/(2U) \tag{13}$$

where α_0 is the angle of attack at zero lift needed for chambered airfoils. Note that the acceleration terms of the added mass are neglected in this expression, because they for moderate reduced frequencies are an order lower than the pitch-rate term. The term $\frac{c\,\dot{U}}{2\,U^2}$ in the differential equation (11) for the states x_1 and x_2 has the same order as the reduced frequency, thus it can also be neglected if the reduced frequency is small compared to the non-dimensional time constants b_1 and b_2. In that case, the present model reduces to the original B-L model where the effect of time-varying free-stream velocity is neglected.

Stalled flow with trailing edge separation

The B-L model deals with both LE and TE separation. The LE separation is not included in the present model because it is not a dominating phenomenon for wind turbine applications, where the airfoils have thicknesses of no less than 15 %. Furthermore, the modelling of the vortex travel during LE separation requires that the time of the vortex shedding is marked on an additional time-scale, whereby the model becomes implicit and impractical for stability analysis.

The basic assumption in the B-L model of TE separation is that the static lift curve can be represented by the expression

$$C_L^{\mathrm{st}} = C_{L,\alpha}\left(\frac{1 + \sqrt{f^{\mathrm{st}}(\alpha)}}{2}\right)^2 (\alpha - \alpha_0) \tag{14}$$

which is the lift on a flat plate in a potential Kirchhoff flow [20]. The constant $C_{L,\alpha}$ is the slope of the lift curve in the linear region of attached flow, and the function $f^{\mathrm{st}}(\alpha)$ determines the separation point for the TE separation as defined in Figure 2. The flow is fully attached for $f = 1$ and fully separated for $f = 0$.

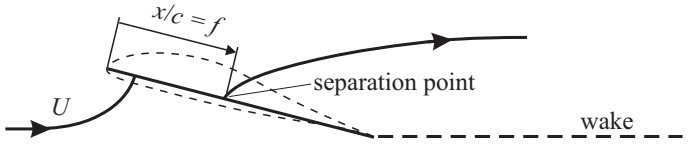

Figure 2. The trailing edge separation point f defined in the Kirchhoff flow past a flat plate.

Assuming that the static lift curve is given, the separation point can be determined as function of angle of attack by inversion of Equation (14)

$$f^{\mathrm{st}} = \left(2\sqrt{\frac{C_L^{\mathrm{st}}(\alpha)}{C_{L,\alpha}(\alpha-\alpha_0)}} - 1\right)^2 \tag{15}$$

There are two issues of this inversion and the representation of the lift curve by (14) that must be handled. First, the separation point cannot exceed the LE of the airfoil, $f^{\mathrm{st}} \leq 1$, the linear lift slope is therefore defined as

$$C_{L,\alpha} = \max\{C_L^{\mathrm{st}}(\alpha)/(\alpha-\alpha_0)\} \tag{16}$$

for all angles of attack in the attached flow region. Usually, lift curves provided as input to the model have a range of low angles of attack where they are completely linear and a slope given by (16). However, in cases where lift curves are provided directly from measurements, or CFD computations, it can be necessary to use linear regression to determine a linear lift curve in a range of lower angles of attack with fully attached flow.

Second, the two angles of attack $\alpha^{+\mathrm{fs}}$ and $\alpha^{-\mathrm{fs}}$ at full separation $f^{\mathrm{st}}(\alpha^{\pm\mathrm{fs}}) = 0$ on the upper and lower airfoil surface, respectively, can be determined from the equation $|C_L^{\mathrm{st}}(\alpha^{\pm\mathrm{fs}})| = |C_{L,\alpha}(\alpha^{\pm\mathrm{fs}} - \alpha_0)/4|$. Beyond these angles of attack the static lift curve cannot be represented by expression (14), and the separation point function is set to zero $f^{\mathrm{st}} = 0$.

To handle variations in α exceeding the limits of full separation, the static lift curve is represented by a linear interpolation between lift coefficients for fully attached and fully separated flow

$$C_L^{\mathrm{st}} = C_{L,\alpha}(\alpha-\alpha_0)\, f^{\mathrm{st}} + C_L^{\mathrm{fs}}(\alpha)\,(1-f^{\mathrm{st}}) \tag{17}$$

where the lift coefficient for fully separated flow is computed as

$$C_L^{\mathrm{fs}} = \frac{C_L^{\mathrm{st}} - C_{L,\alpha}(\alpha-\alpha_0)\, f^{\mathrm{st}}}{1-f^{\mathrm{st}}} \tag{18}$$

from the static lift curve C_L^{st} and the separation point function f^{st} defined by (15). This function equals the static lift curve beyond the angles of attack $\alpha^{\pm\mathrm{fs}}$ where the flow becomes fully separated ($f^{\mathrm{st}} = 0$).

Note that Equation (18) poses a problem for the angles of attack in the fully attached region where $f^{\mathrm{st}} = 1$. However, by substitution of the separation point function (15) into (18), it can be shown that

$$C_L^{\mathrm{fs}}(\alpha) \to \frac{C_L^{\mathrm{st}}(\alpha)}{2} \quad \text{when} \quad f^{\mathrm{st}} \to 1 \quad \text{for} \quad C_{L,\alpha}(\alpha-\alpha_0) \to C_L^{\mathrm{st}}(\alpha) \tag{19}$$

Hence, the lift for fully separated flow at low angles of attack is half the lift for fully attached flow.

Figure 3 shows an example of a static lift curve represented by the interpolation (17). The method for obtaining this representation of C_L^{st} is: Find the angle of zero lift α_0 and the maximum linear lift slope $C_{L,\alpha}$, then compute the separation point function f^{st} from (15) using the original lift curve, and finally compute the lift coefficient for fully separated flow C_L^{fs} from (18).

Dynamics of trailing edge separation

Two state variables in the B-L model are used to describe the dynamic behavior of TE separation. The separation is related to the pressure distribution over the airfoil, and the pressure is related to lift on the airfoil; for a certain lift there is a certain pressure distribution with a certain separation point. It is assumed that there is a time-lag between the pressure and lift, modelled as

$$\dot{x}_3 + T_p^{-1} x_3 = T_p^{-1} C_L^p(t) \tag{20}$$

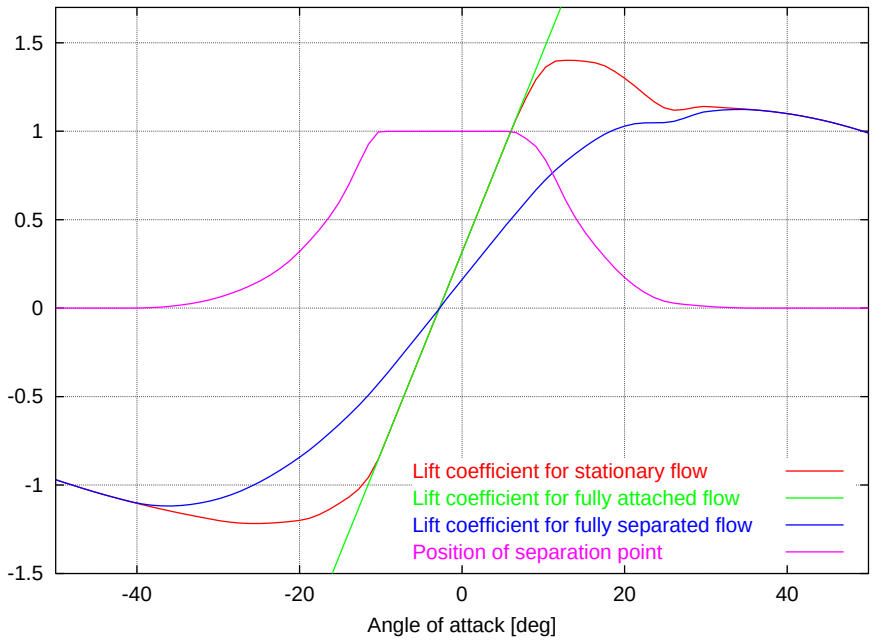

Figure 3. Example of a static lift curve represented by the interpolation (17)*, where the lift coefficient for fully separated flow is obtained by* (18) *and the separation point function is obtained by* (15) *using the original static lift curve.*

where $C_L^p(t)$ is the unsteady lift coefficient for attached flow given by (13), and T_p is the time constant for the pressure lag. The initial condition is $x_3(0) = 0$.

The state variable x_3 is a lift coefficient $C_L^{p\prime} = x_3(t)$ with a time-lag to the actual lift coefficient C_L^p for attached flow. This coefficient determines an equivalent angle of attack that gives the same quasi-steady lift: $\alpha_f = C_L^{p\prime}/C_{L,\alpha} + \alpha_0$. For this angle of attack, an equivalent quasi-steady separation point $f' = f^{\mathrm{st}}(\alpha_f)$ can be obtained from Equation (15).

The second state variable of the TE separation arises due to dynamics of the boundary layer, which causes the separation point to lag behind the quasi-steady value f' as described by the equation

$$\dot{x}_4 + T_f^{-1} x_4 = T_f^{-1} f'(t) \tag{21}$$

where T_f is a time constant for the lag in the boundary layer, and $x_4(0) = 0$. The variable x_4 is the fourth and last state variable of the present model. Using (17), the unsteady separation point $f'' = x_4(t)$ determines the unsteady lift coefficient that includes the effect of TE separation

$$C_L^{\mathrm{dyn}} = C_{L,\alpha}(\alpha_E - \alpha_0)\, f'' + C_L^{\mathrm{fs}}(\alpha_E)\,(1 - f'') + \pi T_u \dot{\alpha} \tag{22}$$

where the added mass term from (13) related to the pitch rate is included, and the time constant

$$T_u = \frac{c}{2U} \tag{23}$$

has been introduced. Note that this quantity is not constant in time due to the time-varying flow velocity $U = U(t)$.

The total unsteady lift on an airfoil under the attached and stalled flow conditions can now be determined from Equation (22) by simultaneous solution of the state equations (11), (20), and (21). The direction of the unsteady lift force is assumed to be perpendicular to the effective angle of attack α_E.

2.2 Drag

The model for unsteady drag differs from the original B-L model in the way that the unsteady drag is bounded to variations about the static drag curve provided as input to the model, which is the method used in the previous implementation in the aeroelastic code HAWC [1, 2]. The drag is considered to consist of basically two parts: *Induced drag* and *viscous drag*. Induced drag is caused by angle shift of the effective lift force due to the downwash induced by the wake. Viscous drag is caused by the viscous boundary layer and consists of friction and pressure drag. The two types are now introduced into the model.

Induced drag

Induced drag is caused by the shift of the unsteady lift angle due to the wake downwash. It is always present for wings with finite span because of the tip vortices and the resulting trailing edge vortex shedding. However, when modelling an airfoil in two dimensions induced drag is an unsteady phenomenon only.

Under steady conditions (the airfoil is not moving and inflow is constant), the circulation on the airfoil is constant, no wake is shed, and the aerodynamic force is perpendicular to the geometric angle of attack. Under unsteady conditions, the induction of the shed wake yields that the effective angle of attack α_E is lagging behind the geometric angle of attack α. The unsteady lift force is perpendicular to α_E, and thereby has a component in the drag direction defined by the geometric angle of attack. This phenomenon is illustrated in Figure 4. The induced drag coefficient is assumed to be given by

$$\Delta C_D^{\mathrm{ind}} = (\alpha - \alpha_E)\, C_L^{\mathrm{dyn}} \tag{24}$$

where α_E and C_L^{dyn} are computed from (12) and (22), respectively. The geometric angle of attack α is computed as the angle between the chord and the free-stream flow, including the airfoil motion.

Viscous drag

The viscous drag originates from the boundary layer. Under attached flow conditions it can be characterized as friction drag. The friction drag vary little with angle of attack, and gives an almost steady contribution to the total drag; any unsteadiness is due to fluctuations in transition between the laminar and turbulent boundary layer. When the TE separation develops, there is a large increase in the viscous drag due to pressure drag. The pressure in separated boundary layer is lower than in the attached boundary layer upstream, which by summation yields a force component in the drag direction.

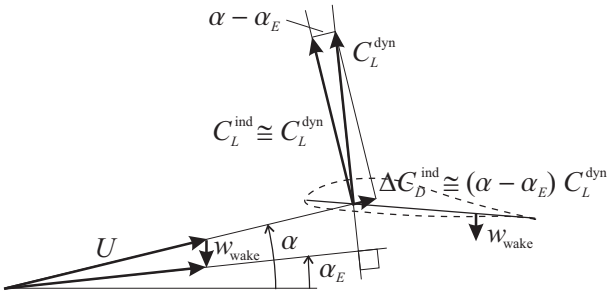

Figure 4. Induced drag is caused by the shift of the unsteady lift angle due to the wake downwash.

In the B-L model, the unsteadiness of the pressure drag due to the variations in TE separation point f is deduced from the analytical expression for the pressure drag on a flat plate in a potential Kirchhoff flow [20]. Similar to the expression for the lift (14), this expression is

$$C_D^{\text{Kirchhoff}} = C_{L,\alpha}\alpha^2 \left(\frac{1-\sqrt{f}}{2}\right)^2 \tag{25}$$

It shows that the pressure drag for this flow is the product $C_{L,\alpha}\alpha^2$ weighted with the separation point dependent factor $(1-\sqrt{f})^2/4$. Beddoes and Leishman [11] notes that expression (25) *does not give a favorable comparison with experimental test except for minor separations*. The B-L model therefore applies an alternative procedure, however still based on Kirchhoff's result.

In the present model, it is assumed that the factor $(1-\sqrt{f})^2/4$ describes the relative variation of the pressure drag due to variation of separation point. The unsteady contribution to the total drag because the unsteady separation point f'' lags behind the separation point for the effective angle of attack α_E is therefore assumed to be given by

$$\Delta C_D^{f''} = \left(C_D^{\text{st}}(\alpha_E) - C_{D_0}\right)\left(\left(\frac{1-\sqrt{f''}}{2}\right)^2 - \left(\frac{1-\sqrt{f^{\text{st}}(\alpha_E)}}{2}\right)^2\right) \tag{26}$$

where the function C_D^{st} is the static drag curve, and the constant C_{D_0} is the drag coefficient at zero lift describing the friction drag. The term $C_D^{\text{st}} - C_{D_0}$ substitutes the product $C_{L,\alpha}\alpha^2$ in original Kirchhoff's expression, and it describes the order of the pressure drag.

The total unsteady drag coefficient is assumed to be given by

$$C_D^{\text{dyn}} = C_D^{\text{st}}(\alpha_E) + \Delta C_D^{\text{ind}} + \Delta C_D^{f''} \tag{27}$$

where the first term ensures that the unsteady drag is bounded to the static drag curve C_D^{st}, and the remaining two terms describe the unsteadiness of the induced drag and pressure drag, respectively. For steady state conditions ($f'' \to f^{\text{st}}$ and $\alpha_E \to \alpha$) the unsteady drag coefficient (27) equals the static drag coefficient because $\Delta C_D^{\text{ind}} \to 0$ and $\Delta C_D^{f''} \to 0$.

2.3 Moment

The model of the unsteady pitching moment has some similarity with the original B-L model, where the unsteady TE separation affects the moment through the travelling of the pressure center due to the separation. However as for the drag, the present model binds the unsteady moment to variations about the static moment curve provided as input. The unsteady moment coefficient is approximated by

$$C_M^{\text{dyn}} = C_M^{\text{st}}(\alpha_E) + \Delta C_M^{f''} - \pi c\,\dot{\alpha}/(4U) \tag{28}$$

where C_M^{st} is the static moment curve, $\Delta C_M^{f''}$ is the unsteady moment due to the dynamic TE separation, and the last term is the added mass effect that arises from the pitch rate of the airfoil. Note that the sign of this term defines the so-called *pitch rate damping*, which is important for prediction of classical flutter.

To model the effect of TE separation on the moment it is assumed that there is a relation between the separation point and the position of the pressure center. Figure 5 illustrates how the position of an equivalent pressure center can be defined by the static lift and moment curves as

$$a^{\text{st}} = \frac{C_M^{\text{st}} - C_{M_0}}{C_L^{\text{st}}} \tag{29}$$

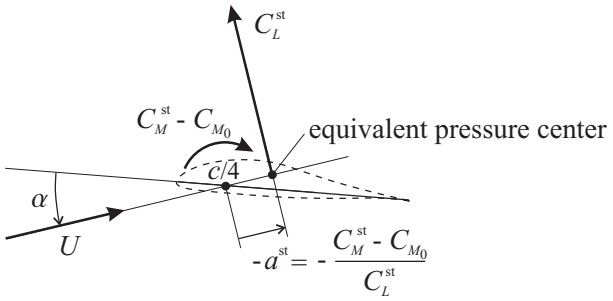

Figure 5. Definition of the distance a^{st} from the quarter-chord to the equivalent pressure center.

where the constant C_{M_0} is the moment coefficient at zero lift. The arm of the lift force a^{st} is the distance from the quarter chord point to the equivalent pressure center where the lift C_L^{st} is acting to give the moment $C_M^{\mathrm{st}} - C_{M_0}$. Strictly, the normal coefficient C_N should be used to compute the displacement of the pressure center on the chord, however, the angles of attack where the trailing edge separation point moves over the airfoil are moderate $|\alpha^{\pm \mathrm{fs}}| \sim 35°$.

The arm a^{st} given by (29) is assumed to be directly related to the separation point f^{st} given by expression (15). Figure 6 shows how a^{st} changes with f^{st} for TE separation on the upper and lower airfoil surface. The airfoil data is the same as used for Figure 3. It is taken from the aerodynamic input to an aeroelastic wind turbine code, where accurate description of the pitching moment is not a main priority, especially for negative angles of attack. This may explain the noticeable difference between the behavior of the two types of TE separation. For a symmetrical airfoil there is no discontinuity of the pressure center position going over the attached flow region from upper to lower surface TE separation. For cambered airfoils there may be this difference in arm, where it may be most consistent to define two functions for a^{st}. However, because airfoils on a wind turbine blade mainly operates at positive angles of attack the function a^{st} is herein based on a cubic spline fit to the data for the TE separation on the upper surface only.

From the relation between pressure center and TE separation point, it is assumed that the unsteady moment coefficient due to the dynamic variations of the separation point can be described as

$$\Delta C_M^{f''} = C_L^{\mathrm{dyn}} \left(a^{\mathrm{st}}(f'') - a^{\mathrm{st}} \left(f^{\mathrm{st}}(\alpha_E) \right) \right) \tag{30}$$

where f'' is the unsteady position of the separation point, and C_L^{dyn} is the dynamic lift coefficient given by Equation (22).

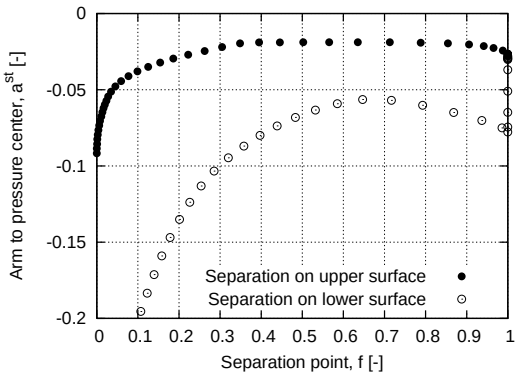

Figure 6. Distance of the equivalent pressure center as function of the point of TE separation on the upper and lower surface of the same airfoil as in Figure 3.

2.4 Closed set of nonlinear equations

The state-space formulation of the suggested B-L type dynamic stall model is here summarized by presenting the closed set of coupled equations. These nonlinear ordinary differential equations (ODEs) will be coupled in aeroelastic models with the structural equations for the airfoil motion.

Figure 7 illustrates the flow of variables in this coupled aeroelastic system. Structural and aerodynamic equations of this system must be solved simultaneously, however in this presentation the airfoil motion is assumed to be prescribed. Hence, the geometric angle of attack α, the pitch-rate $\dot{\alpha}$, the angle of attack at the three-quarter point $\alpha_{3/4}$, and the time-varying free-stream velocity U are given explicit by prescribed structural states.

The differential equations of the dynamic stall model are given by (11), (20), and (21), which are coupled through different algebraic equations. The coupled set of nonlinear ODEs can be rewritten as

$$\begin{aligned}
\dot{x}_1 + T_u^{-1}\left(b_1 + c\,\dot{U}/(2\,U^2)\right) x_1 &= b_1 A_1 T_u^{-1}\,\alpha_{3/4} \\
\dot{x}_2 + T_u^{-1}\left(b_2 + c\,\dot{U}/(2\,U^2)\right) x_2 &= b_2 A_2 T_u^{-1}\,\alpha_{3/4} \\
\dot{x}_3 + T_p^{-1} x_3 &= T_p^{-1}\left(C_{L,\alpha}\,(\alpha_E - \alpha_0) + \pi T_u\,\dot{\alpha}\right) \\
\dot{x}_4 + T_f^{-1} x_4 &= T_f^{-1} f^{\mathrm{st}}\left(x_3/C_{L,\alpha} + \alpha_0\right)
\end{aligned} \tag{31}$$

where the initial conditions are $x_i(0) = 0$. The effective angle of attack α_E is linear dependent on x_1 and x_2 as given by (12). Note that the time constant $T_u = c/(2U(t))$ is time-varying due to the dependency on the structural states through the free-stream velocity U.

The unsteady aerodynamic coefficients are given by

$$\begin{aligned}
C_L^{\mathrm{dyn}} &= C_{L,\alpha}(\alpha_E - \alpha_0)\,x_4 + C_L^{\mathrm{fs}}(\alpha_E)\,(1 - x_4) + \pi T_u\,\dot{\alpha} \\
C_D^{\mathrm{dyn}} &= C_D^{\mathrm{st}}(\alpha_E) + (\alpha - \alpha_E)\,C_L^{\mathrm{dyn}} \\
&\quad + \left(C_D^{\mathrm{st}}(\alpha_E) - C_{D_0}\right)\left(\frac{\sqrt{f^{\mathrm{st}}(\alpha_E)} - \sqrt{x_4}}{2} - \frac{f^{\mathrm{st}}(\alpha_E) - x_4}{4}\right) \\
C_M^{\mathrm{dyn}} &= C_M^{\mathrm{st}}(\alpha_E) + C_L^{\mathrm{dyn}}\left(a^{\mathrm{st}}(x_4) - a^{\mathrm{st}}\left(f^{\mathrm{st}}(\alpha_E)\right)\right) - \frac{\pi}{2} T_u\,\dot{\alpha}
\end{aligned} \tag{32}$$

where f^{st}, $C_{L,\alpha}$, C_L^{fs}, and a^{st} are defined by (15), (16), (18), and (29), respectively.

Equations (31) and (32) form a closed set of coupled nonlinear equations. These equations govern the unsteady forces on an airfoil, and can directly be used together with a Blade Element Momentum method in an aeroelastic code for wind turbines. However as noted by Leishman and Crouse in [15], the system has a tendency to be *stiff* which complicates a numerical integration. Hence, for nonlinear time-domain analysis it is still preferable to use the indicial function formulation of the model as shown in Section 3. The purpose of the state-space formulation is

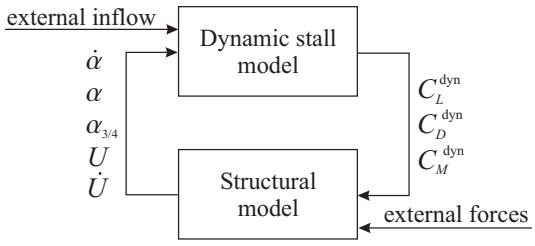

Figure 7. Schematics of the coupled aeroelastic system showing the variable flow.

to enable stability analysis; it is therefore shown in the next section how the set of equations can by linearized for small amplitude vibrations of the airfoil about a steady-state equilibrium.

2.5 Linearization about a steady state

Wind turbines do not exhibit steady state behavior during operation due to air turbulence, wind shear, gravitational excitation, tower shadow, and other effects. However, to give a first order approximation to the dynamic behavior of turbines, these effects can be neglected by assuming that the turbine is operating in a steady state equilibrium between aerodynamic and structural forces.

To analyze the stability of this equilibrium, the dynamic stall model is now linearized assuming small amplitude vibrations about an equilibrium

$$\alpha(t) = \alpha^0 + \epsilon\,\alpha^1(t)\ ,\quad \alpha_{3/4}(t) = \alpha^0 + \epsilon\,\alpha^1_{3/4}(t)\ ,\quad U(t) = U_0 + \epsilon\,U_1(t) \tag{33}$$

where the equilibrium is given by the steady angle of attack α^0 and the mean free-stream velocity U_0. The vibrations about this equilibrium state is given by the perturbations α^1, $\alpha^1_{3/4}$, and U_1, which are small as indicated by the book-keeping parameter $\epsilon \ll 1$.

A perturbation solution to the state equations (31) is sought on the form

$$x_i(t) = x_i^0 + \epsilon\,x_i^1(t) \quad \text{for} \quad i = 1,2,3,4 \tag{34}$$

where x_i^0 is the steady state and x_i^1 is a small perturbation of the dynamic stall variables. Insertion of (33) and (34) into (31), and evaluation of the ϵ^0-order equations, the steady states become

$$x_1^0 = A_1\alpha^0,\quad x_2^0 = A_2\alpha^0,\quad x_3^0 = C_{L,\alpha}\left(\alpha^0 - \alpha_0\right),\quad x_4^0 = f^{\rm st}\left(\alpha^0\right) \tag{35}$$

The ϵ^1-order equations with substitution of these steady states become

$$\begin{aligned}
\dot{x}_1^1 + T_1^{-1}x_1^1 &= T_1^{-1}A_1\,\alpha^1_{3/4}(t) - \frac{A_1\alpha^0}{U_0}\,\dot{U}_1(t)\\
\dot{x}_2^1 + T_2^{-1}x_2^1 &= T_2^{-1}A_2\,\alpha^1_{3/4}(t) - \frac{A_2\alpha^0}{U_0}\,\dot{U}_1(t)\\
\dot{x}_3^1 + T_p^{-1}x_3^1 &= T_p^{-1}\left(C_{L,\alpha}\alpha_E^1 + \pi T_0\,\dot{\alpha}^1(t)\right)\\
\dot{x}_4^1 + T_f^{-1}x_4^1 &= T_f^{-1}\left.\frac{df^{\rm st}}{d\alpha}\right|_{\alpha=\alpha^0}\frac{x_3^1}{C_{L_\alpha}}
\end{aligned} \tag{36}$$

where two new time constants are introduced as $T_i = T_0/b_i$ with $T_0 = c/(2U_0)$, and $\alpha_E^1 = \alpha^1_{3/4}\phi(0) + x_1^1 + x_2^1$ is the linear effective angle of attack (cf. Equation (12)). The linearization of the fourth equation is performed by Taylor expanding the separation point function $f^{\rm st}$ about the steady angle of attack α^0, where the derivative of $f^{\rm st}$ can be derived from expression (15) as

$$\frac{df^{\rm st}}{d\alpha} = \frac{2}{C_{L,\alpha}(\alpha-\alpha_0)}\left(\frac{dC_L^{\rm st}}{d\alpha} - \frac{C_L^{\rm st}(\alpha)}{\alpha-\alpha_0}\right)\left(2 - \sqrt{\frac{C_{L,\alpha}(\alpha-\alpha_0)}{C_L(\alpha)}}\right) \tag{37}$$

The linear equations (36) are the governing equations for the linearized dynamic stall model. Solution of these equations for $x_i^1(0) = 0$ yields the linear approximations to the aerodynamic states.

To obtain a completely linearized model, the aerodynamic coefficients (32) are also linearized using Taylor expansion about the steady state equilibrium

$$\begin{aligned}
C_L^{\rm lin} &= C_L^0 + c_{l,\alpha}\,\alpha_E^1 + c_{l,f}\,x_4^1 + \pi T_0\,\dot{\alpha}^1(t)\\
C_D^{\rm lin} &= C_D^0 + c_{d,\alpha}\,\alpha_E^1 + c_{d,f}\,x_4^1 + C_L^0\left(\alpha^1(t) - \alpha_E^1\right)\\
C_M^{\rm lin} &= C_M^0 + c_{m,\alpha}\,\alpha_E^1 + c_{m,f}\,x_4^1 - \frac{\pi}{2}T_0\,\dot{\alpha}^1(t)
\end{aligned} \tag{38}$$

where the coefficients are given by

$$
\begin{aligned}
c_{l,\alpha} &= C_{L,\alpha} f_0 + \left.\frac{dC_L^{\mathrm{fs}}}{d\alpha}\right|_{\alpha=\alpha^0} (1-f_0) \\
c_{l,f} &= C_{L,\alpha}(\alpha^0 - \alpha_0) - C_L^{\mathrm{fs}}(\alpha^0) \\
c_{d,\alpha} &= \left.\frac{dC_D}{d\alpha}\right|_{\alpha=\alpha^0} - \left.\frac{df^{\mathrm{st}}}{d\alpha}\right|_{\alpha=\alpha^0} (C_{D_0} - C_D^0)\frac{1-\sqrt{f_0}}{4\sqrt{f_0}} \\
c_{d,f} &= (C_{D_0}^{\mathrm{st}} - C_D^0)\frac{1-\sqrt{f_0}}{4\sqrt{f_0}} \\
c_{m,\alpha} &= \left.\frac{dC_M^{\mathrm{st}}}{d\alpha}\right|_{\alpha=\alpha^0} - C_L^0 \left.\frac{df^{\mathrm{st}}}{d\alpha}\right|_{\alpha=\alpha^0} \left.\frac{da^{\mathrm{st}}}{df}\right|_{\alpha=\alpha^0} \\
c_{m,f} &= C_L^0 \left.\frac{da^{\mathrm{st}}}{df}\right|_{\alpha=\alpha^0}
\end{aligned}
\tag{39}
$$

and C_L^0, C_D^0, and C_M^0 are the static lift, drag, and moment coefficients at the steady state angle of attack α^0. The derivative of C_L^{fs} can be derived as

$$
\frac{dC_L^{\mathrm{fs}}}{d\alpha} = \frac{\left(\frac{dC_L}{d\alpha} - C_{L,\alpha} f^{\mathrm{st}}(\alpha)\right)(1 - f^{\mathrm{st}}(\alpha)) + (C_L - C_{L,\alpha}(\alpha - \alpha_0))\frac{df^{\mathrm{st}}}{d\alpha}}{(1 - f^{\mathrm{st}}(\alpha))^2} \tag{40}
$$

and the derivative of a^{st} is computed from the cubic spline.

There are some problems with singularities in the linearization for an airfoil in a fully attached ($f_0 = 1$), or fully separated ($f_0 = 0$) flow, which must be considered when computing the coefficients (39). For $f_0 = 1$ the derivative of the lift coefficient for fully separated flow must be computed as $dC_L^{\mathrm{fs}}/d\alpha = \frac{1}{2} dC_L^{\mathrm{st}}/d\alpha$, where the limit given in Equation (19) has been used. For $f_0 = 0$ the coefficients for the linear drag must computed as $c_{d,\alpha} = \left.\frac{dC_D}{d\alpha}\right|_{\alpha=\alpha^0}$ and $c_{d,f} = 0$ to avoid singularities by dividing with zero. The simplification of the first coefficient is given by the fact that $df^{\mathrm{st}}/d\alpha = 0$ for $f_0 = 0$. The second coefficient $c_{d,f}$ can be set to zero because it has no effect on the linear drag when the flow is fully separated where the perturbed unsteady separation point variable x_4^1 will be zero due to $df^{\mathrm{st}}/d\alpha = 0$, as seen in Equation (36).

3 Indicial formulation

In this section, the differential equations describing the dynamic stall model are rewritten to an implicit indicial method formulation to facilitate effective numerical solution of the aeroelastic equations in the context of full aeroelastic models.

When the response of a driving force for a linear system, such as the present dynamic stall model, is sought, Duhamels integral can be employed. A case that is very numerically efficient occurs when the response of the system can be expressed in terms of exponential functions, in which case the solution of each of the state-variables for each time-step is reduced to decaying the value from the previous time-step and adding a new increment.

To have the same basis of the formulation for the present model in both the state space and indicial formulations, an indicial formulation of the model equations (31) is derived below.

3.1 General considerations

The differential equations of the model are linear first order equations

$$\dot{x}_i + P_i x_i = Q_i, \tag{41}$$

where index i describes the number of the equation, and the coefficients P_i and Q_i in the general case are time-varying. The solution to this general differential equation at time $t = t_e$ is

$$x_i(t_e) = \int_{t_s}^{t_e} Q_i e^{-\int_t^{t_e} P_i d\tau} dt + x_i(t_s) \tag{42}$$

where t_s is the initial time. The solution at time $t = t_e + \Delta t$ is

$$\begin{aligned} x_i(t_e + \Delta t) &= \int_{t_s}^{t_e+\Delta t} Q_i e^{-\int_t^{t_e+\Delta t} P_i d\tau} dt + x_i(t_s) \\ &= e^{-\int_{t_e}^{t_e+\Delta t} P_i dt} \int_{t_s}^{t_e} Q_i e^{-\int_t^{t_e} P_i d\tau} dt \\ &\quad + \int_{t_e}^{t_e+\Delta t} Q_i e^{-\int_t^{t_e+\Delta t} P_i d\tau} dt + x_i(t_s), \end{aligned} \tag{43}$$

With initial conditions $x_i(t_s) = 0$, Equations (42) and (43) shows that the solution at the next time step can be written as

$$x_i(t_e + \Delta t) = C_{dec,i}\, x_i(t_e) + I_{new,i}. \tag{44}$$

where

$$C_{dec,i} = e^{-\int_{t_e}^{t_e+\Delta t} P_i dt} \tag{45}$$

$$I_{new,i} = \int_{t_e}^{t_e+\Delta t} Q_i e^{-\int_t^{t_e+\Delta t} P_i d\tau} dt. \tag{46}$$

These time-varying coefficients are the decay ($C_{dec,i}$) and the increment ($I_{new,i}$) due to the right-hand side of Equation (41).

3.2 Discretization

Several strategies can be employed when solving the general equations, the most simple one being the assumption of piecewise constant P_i and Q_i values.

Piecewise constant terms

Under this assumption, the decay and increment reduces to

$$C_{dec,i}^{const} = e^{-\bar{P}_i \Delta t} \tag{47}$$

$$I_{new,i}^{const} = \frac{\bar{Q}_i}{\bar{P}_i}(1 - e^{-\bar{P}_i \Delta t}). \tag{48}$$

The constant values can be approximated using the midpoint values

$$\bar{P}_i^j = 0.5(P_i^{j-1} + P_i^j) \tag{49}$$

$$\bar{Q}_i^j = 0.5(Q_i^{j-1} + Q_i^j) \tag{50}$$

Note that the superscripts and subscripts on P and Q refer to time step index and state variables, respectively. The coefficients in the expressions above are for the state variables $i = 1$ and $i = 2$ given as

$$\bar{P}_i^j = b_i \frac{U^j + U^{j-1}}{c} + \frac{\dot{U}^j + \dot{U}^{j-1}}{U^j + U^{j-1}}, \tag{51}$$

$$\bar{Q}_i^j = \frac{b_i A_i}{c} \left(U^{j-1} \alpha_{3/4}^{j-1} + U^j \alpha_{3/4}^j \right) \tag{52}$$

whereas the coefficients for the state variables $i = 3$ and $i = 4$ are

$$\bar{P}_3^j = T_p^{-1} \tag{53}$$

$$\bar{Q}_3^j = 0.5\ T_p^{-1} \Big[C_{L,\alpha} (\alpha_E^{j-1} + \alpha_E^j - 2\alpha_0) + \frac{\pi c}{2} \left(\dot{\alpha}^{j-1} / U^{j-1} + \dot{\alpha}^j / U^j \right) \Big] \tag{54}$$

$$\bar{P}_4^j = T_f^{-1} \tag{55}$$

$$\bar{Q}_4^j = 0.5\ T_f^{-1} \left[f_{st}(x_3^{j-1} / C_{L,\alpha} + \alpha_0) + f_{st}(x_3^j / C_{L,\alpha} + \alpha_0) \right] \tag{56}$$

Higher order discretizations

More accurate and elaborate formulas may be derived under the assumptions of linear or parabolic P_i and Q_i in time. The expressions, however, become very complex, involving error functions, if P_i is not assumed piecewise constant. Under the assumption of piecewise constant P_i combined with linear and parabolic Q_i in time, the decay and increments are

$$C_{dec,i}^{linQ} = C_{dec,i}^{const} \tag{57}$$

$$I_{new,i}^{linQ} = \frac{Q_i^{j-1}}{\bar{P}_i^j}(1 - e^{-\bar{P}_i^j \Delta t}) + \frac{Q_i^j - Q_i^{j-1}}{\Delta t \bar{P}_i^j} \left(\Delta t - \frac{1}{\bar{P}_i^j}(1 - e^{-\bar{P}_i^j \Delta t}) \right) \tag{58}$$

$$C_{dec,i}^{parQ} = C_{dec,i}^{const} \tag{59}$$

$$I_{new,i}^{parQ} = \frac{Q_i^{j-1}}{\bar{P}_i^j}(1 - e^{-\bar{P}_i^j \Delta t}) + \frac{Q_i^j - Q_i^{j-2}}{2\Delta t \bar{P}_i^j} \left(\Delta t - \frac{1}{\bar{P}_i^j}(1 - e^{-\bar{P}_i^j \Delta t}) \right) + \frac{Q_i^j - 2Q_i^{j-1} + Q_i^{j-2}}{2\Delta t^2 \bar{P}_i^j} \left(\Delta t^2 - \frac{2\Delta t}{\bar{P}_i^j} + \frac{2}{(\bar{P}_i^j)^2}(1 - e^{-\bar{P}_i^j \Delta t}) \right) \tag{60}$$

The Q_i^j coefficients in the expressions above are for state variables $i = 1$ and $i = 2$ given as

$$Q_i^j = 2b_i A_i \frac{U^j}{c} \alpha_{3/4}^j \tag{61}$$

whereas the Q_i^j coefficients for state variables $i = 3$ and $i = 4$ are

$$Q_3^j = T_p^{-1} \left(C_{L,\alpha}(\alpha_E^j - \alpha_0) + \pi \frac{c}{2U^j} \dot{\alpha} \right) \tag{62}$$

$$Q_4^j = T_f^{-1} f_{st} \left(\frac{x_3^j}{C_{L,\alpha}} + \alpha_0 \right) \tag{63}$$

As previously, α_E^j and $C_L^{p,j}$ is given by

$$\alpha_E^j = \alpha_{3/4}^j (1 - A_1 - A_2) + x_1^j + x_2^j \tag{64}$$

$$C_L^{p,j} = C_{L,\alpha}(\alpha_E^j - \alpha_0) + \pi \frac{c}{2U^j} \dot{\alpha}^j \tag{65}$$

With the above set of equations it is straightforward to compute the decay and increment of the state variables using equations (47)-(48), (57)-(58) or (59)-(60) in the constant, linear or parabolic assumption of Q_i, respectively. Once the decay and increments are found, the state variables are updated using Equation (44), and the unsteady lift, drag, and moment coefficients are computed using Equation (32) for the new time step $t = t^{j+1} = t^j + \Delta t$.

4 Examples

In this section the various parts of the proposed dynamic stall model are validated, and the effect of the model constants are discussed. The first subsection deals with the nonlinear model, after which the linear model is investigated. The last subsection deals with the effect of airfoil thickness on attached-flow response.

4.1 Validation of the nonlinear model

The validation of the nonlinear model is split up in two phases. First, the results obtained with the general unsteady flat-plate inviscid solver described in Appendix A are compared to the results of the nonlinear model. Secondly, the properties of the full dynamic stall model is investigated.

Flat-plate solutions, potential flow

To verify the implementation of the incompressible, inviscid part of the dynamic stall model governed by the first two of the state variables, the model is tested against results obtained with the algorithm for solving inviscid unsteady flat plate flows, described in Appendix A.

Figure 8 show the comparison of the responses of unsteady flat plate flows computed using the general inviscid unsteady flat plate response solver and the proposed dynamic stall model in the case of harmonic pitching motion, harmonic translatory heaving motion and harmonic translatory streamwise motion.

Results for both the proposed model, with the simplifications in the virtual mass terms, and the model using the complete virtual mass terms are shown. The indicial model including the full virtual mass terms agrees well with the benchmark results of the general inviscid unsteady flat plate response solver for all types of motion despite the very violent motion of the airfoil. The small differences are introduced by the approximation to the flat plate response, cf. Equation 6. More terms can be used to represent the indicial ϕ-function if higher accuracy is required.

The difference between the benchmark results and the results of the proposed indicial model are due to the missing added mass term proportional to $\dot{U}\,\alpha + \ddot{h}_{1/2}$. However, it should be noted that the reduced frequency of 0.2 in these test cases is high compared to typical values for wind turbine applications. In cases with moderate motion, the error introduced by the missing added mass terms is substantially smaller.

Full dynamic stall model

To show the behavior of the full dynamic stall model, the response of a NACA 6315 airfoil undergoing pitching motion is shown in Figure 9. It is seen that the well known characteristics of dynamic loops are captured with the model. In the linear region, the effective slope of the lift-loop is reduced, and the direction of the loop is counterclockwise. The corresponding drag loop is mainly due to the inviscid effect described in Section 2. The loop on the moment curve is caused by the upwash velocity, resulting in the effective angle of attack different from the geometrical one. The lift loop near maximum lift has a very different shape owing to the effects of separation. It is seen that the lift curve has the expected overshoot, whereas the drag and moment curves revolve around the static curves. The lift curves for the stalling cases are both clockwise. For the loop around the highest angle of attack with large separation, the drag and moment curves lie closer to the static curves than in the case near maximum lift.

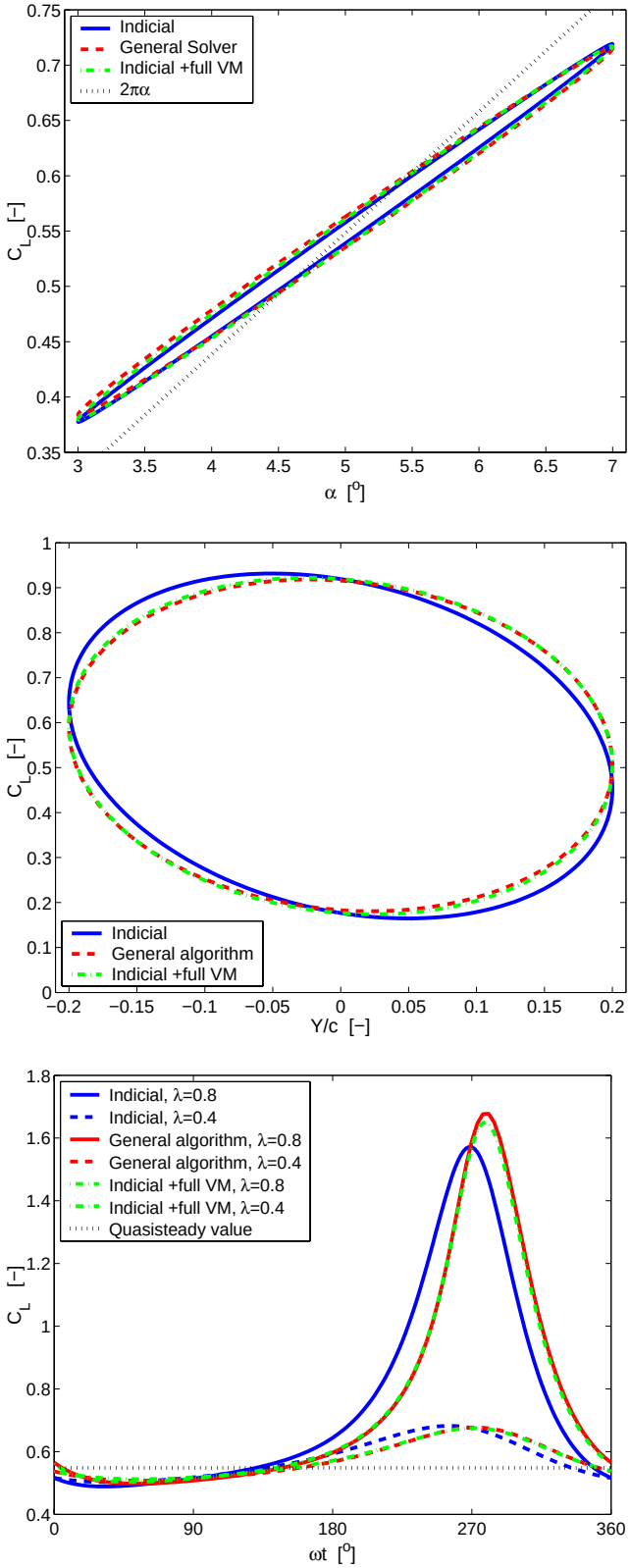

Figure 8. Inviscid response of C_L to oscillatory pitch (upper, $\alpha = 5° \pm 2°$), heave (middle, $y/c = \pm 0.2$ and $\alpha = 5°$) and streamwise motion (lower, $\lambda = A_x \cdot \omega / U_0 = 0.4$ and 0.8; $\alpha = 5°$) for a flat plate. Comparison of results obtained with the general solver described in Appendix A and the indicial model, using both proposed and full virtual mass terms. The reduced frequency is $k = \omega c/(2U_0) = 0.2$ for all results shown.

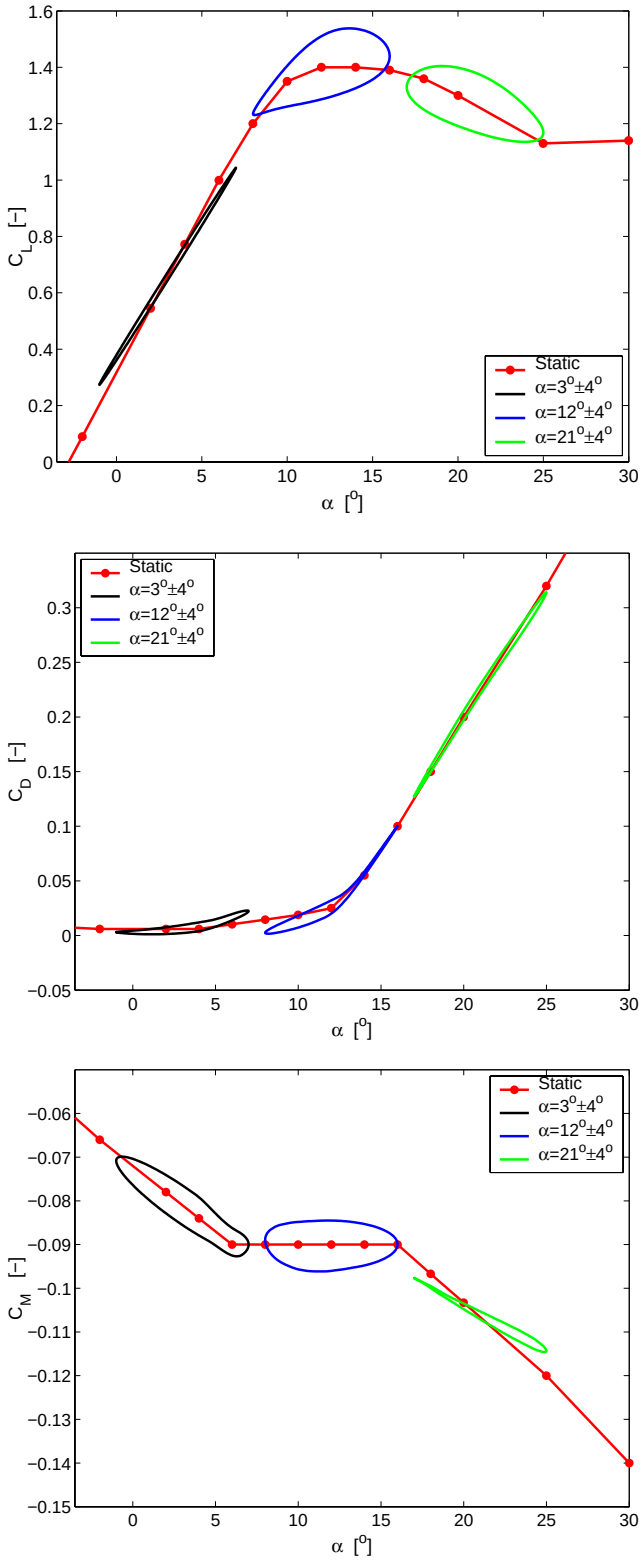

Figure 9. Response of C_L (upper), C_D (middle) and C_M (lower) to oscillatory pitching motion of a NACA 6315 airfoil. Reduced frequency is $k = \omega c/(2U_0) = 0.1$, and the amplitude of the pitching oscillations is $\Delta\alpha = 4°$.

4.2 Validation of the linear model

To validate the performance of the linearized model, Figure 10 show a comparison of the lift, drag and moment responses predicted by the linear and nonlinear version of the model. The left and right figures show the loops for pitch amplitudes of $\Delta\alpha = 4^\circ$ and $\Delta\alpha = 2^\circ$, respectively.

It is seen that the difference between the linear and nonlinear models decreases as the oscillation amplitude decreases. Only slight deviations are present at a pitch amplitudes of $\Delta\alpha = 2^\circ$. For the case of pitch amplitudes of $\Delta\alpha = 1^\circ$, the responses predicted with the linear and nonlinear models were practically identical. This means that the linear model can be applied to determine the linear instabilities of an aeroelastic system [21, 22]. As the motions of the system grows, the nonlinear effects increases, and the nonlinearities may limit the energy input into the system, resulting in limit-cycle oscillations.

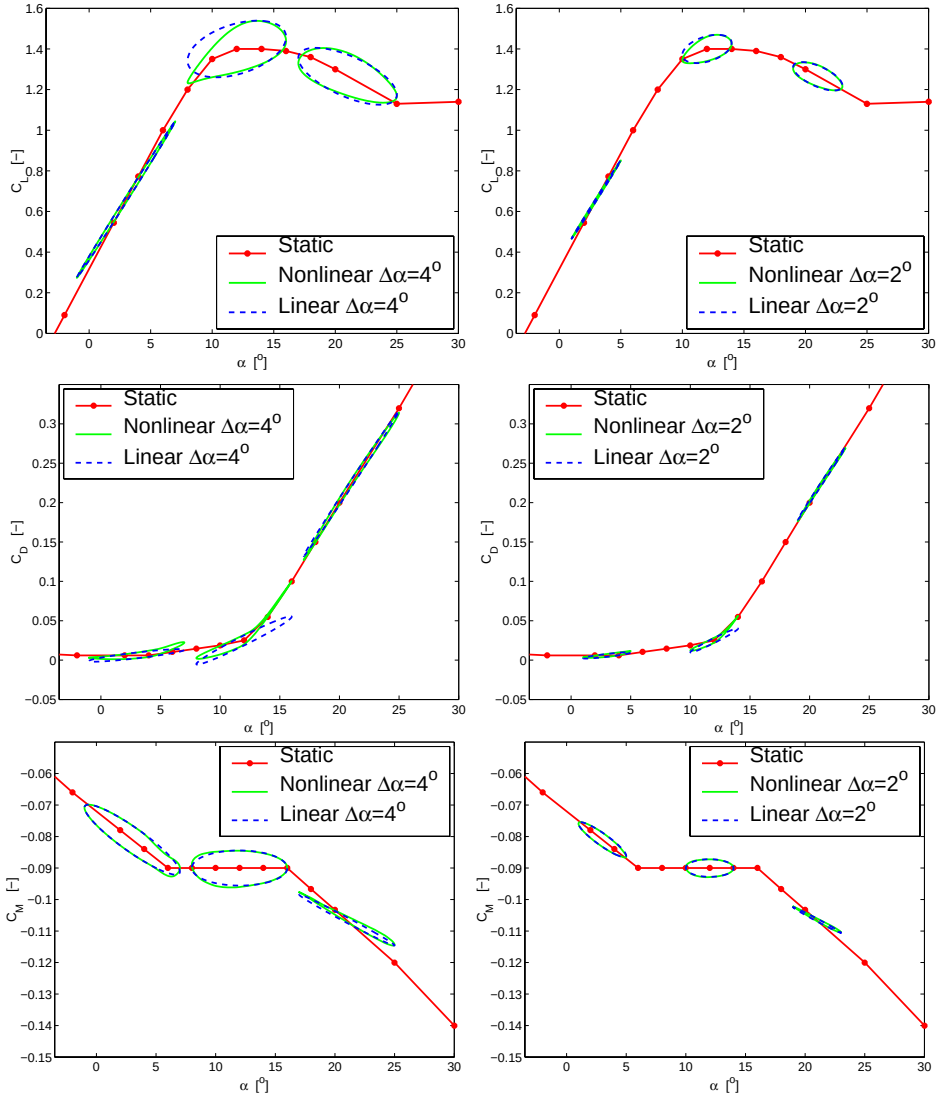

Figure 10. Comparison of responses from the linear and nonlinear model. Response of C_L (upper), C_D (middle) and C_M (lower) to oscillatory pitching motion of a NACA 6315 airfoil. The amplitude of the oscillations is $\Delta\alpha = 4^\circ$ (left) and $\Delta\alpha = 2^\circ$ (right); both with reduced frequency $k = \omega c/(2U_0) = 0.1$.

4.3 Non-zero airfoil thickness, attached flow

The response of a infinitely thin airfoil to a step change in angle of attack was solved by Wagner [23] in 1925. However, the response of an airfoil of finite thickness differs from that of the infinitely thin airfoil [24]. In general the response of non-zero thickness airfoils are lagging that of the zero thickness airfoils.

Figure 11 show the response of the lift to a step change in angle of attack for a flat plate and a Risø A1-24 airfoil. The Risø A1-24 airfoil is a 24% thick airfoil developed specifically for wind turbine applications [25]. The response of the Risø A1-24 airfoil differs significantly from the flat plate response given by the expression by Jones [26], which is the most commonly used approximation to the Wagner function. It is seen from the figure that the response of the thick airfoil is lagging that of the flat plate. The incompressible panel code results are obtained with a code developed by Gaunaa [27].

The commonly used two-term exponential approximation to the Wagner function by Jones approximates the response of the infinitely thin airfoil only, so if the characteristics of the finite thickness airfoil is to be captured correctly, the constants of this two-term exponential approximation must be changed. Using the response of the Risø A1-24 airfoil, an approximate two-term exponential expression was found by minimizing the RMS value of the difference between the approximate expression and the panel code. The obtained approximate response curve is correct to within 1% of the panel code results. The general form of a two-term exponential expression for the response is given by Equation (6). Table 1 lists the coefficients of the two-term exponential approximations to the flat plate and Risø A1-24 airfoil responses.

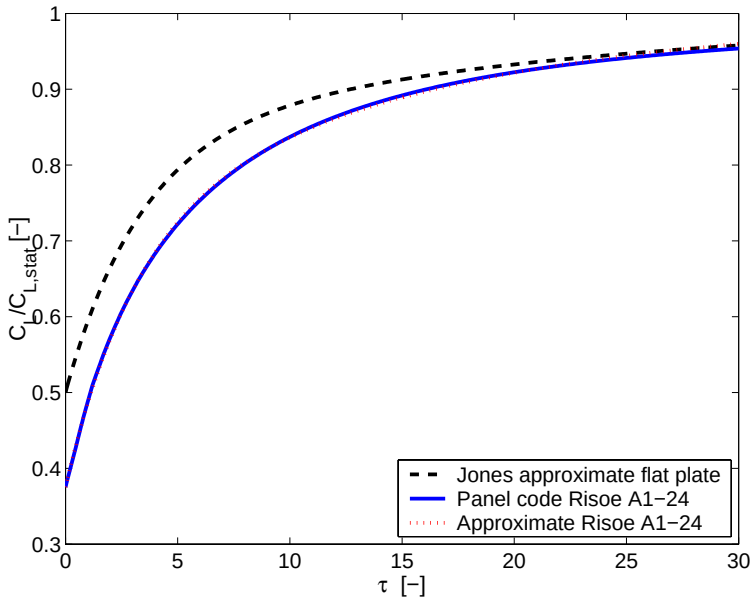

Figure 11. Inviscid response of the lift to a step change in angle of attack for a flat plate and a Risø A1-24 airfoil. $\tau = 2U_0 t/c$

	A_1	A_2	b_1	b_2
Flat plate (Jones [26])	0.165	0.335	0.0455	0.3000
Risø A1-24 airfoil	0.294	0.331	0.0664	0.3266

Table 1. Coefficients for approximate representations of inviscid responses.

The theory leading to the concept of using the downwash in the 3/4 chord point is developed for an infinitely thin airfoil. It is therefore not theoretically proven, that the specific response functions can be employed in the case of airfoils of finite thickness. However, this method yields results in very good agreement with results from Navier-Stokes simulations, which in this respect act as benchmark results. The code used for the Navier-Stokes computations is *EllipSys2D*, developed by Sørensen [28] and Michelsen [29, 30], where the incompressible Reynolds averaged Navier-Stokes equations are solved for the simple variables u, v and p, using a block structured finite volume method. The Navier-Stokes results shown in this work was carried out by F. Bertagnolio from the Wind Energy Department, Risø.

Figure 12 shows the response of a RISØ A1-24 airfoil undergoing pitching oscillations. It is seen that the indicial method results based on the original Wagner-curve approximation by Jones produces results that differs significantly from the Navier-Stokes simulation, and that the indicial method results based on the specific response function for the RISØ A1-24 airfoil is in very good agreement with the Navier-Stokes results.

This shows that it is indeed plausible to use specific response functions if the exact dynamic behavior of a finite thickness airfoil is needed. The small difference between the curves may be explained by viscous effects and the errors introduced by using an approximation for the response function. The dynamic Navier-Stokes results includes an offset on the lift coefficient of $\Delta C_L = -0.016$. This value is chosen such that the mean lift coefficient of the dynamic Navier-Stokes loop is identical to the steady Navier-Stokes lift coefficient at $4.2°$. The reason for the difference between steady and the mean unsteady Navier-Stokes computations is of a numerical nature, but should not affect the dynamic features of the loop.

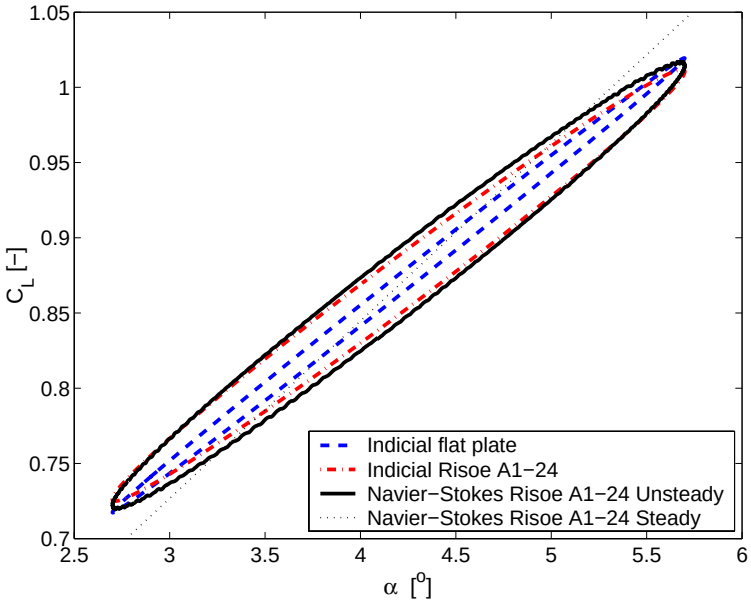

Figure 12. Response from pitching oscillation $\alpha = 4.2° \pm 1.5°$ with a reduced frequency $k = \omega c/(2U_0) = 0.092$ for the RISØ A1-24 airfoil. Comparison between results obtained by Navier-Stokes computations and indicial function formulation using both flat-plate and a specific response function corresponding to the RISØ A1-24 airfoil. The dynamic Navier-Stokes results includes a offset of $\Delta C_L = -0.016$, which accounts for the numerical difference between steady and unsteady Navier-Stokes computations. The zero-lift angle is $\alpha_0 = -3.16°$

5 Conclusion

A new dynamic stall model of the Beddoes-Leishman type intended for wind turbine aeroelasticity has been proposed. Both state-space and indicial formulations are given, as well as, a linearised state-space formulation for aeroelastic stability tools. For wind turbine applications compressibility effects and flow separation initiated from the leading edge are not dominant phenomena, and therefore neglected in the present model. The model includes the effects of shed vorticity from the trailing edge (Theodorsen Theory), and the effects of an instationary trailing edge separation point. As an extension of the original Beddoes-Leishman model, the present model also includes the effect of the time-varying flow velocity on the unsteady lift when an airfoil is vibrating in the streamwise direction, e.g. during stall-induced lead-lag vibrations that can occur for wind turbines.

The only input to the dynamic model is the static lift, drag, and moment curves, four constants determining the unsteady inviscid response (determining two time-constants), and two time-constants determining the unsteady viscous effects.

The dynamic model was compared to unsteady inviscid solutions of flat-plate flows. The comparison of the responses from oscillatory pitching, heaving and lead-lag motion showed very good agreement between the present model and the unsteady inviscid solutions. The proposed dynamic model gives results identical to unsteady inviscid flows within the accuracy of the approximation of the inviscid response function. In the stall region, the model exhibits the expected dynamic features, including the well-known overshoot of the lift when undergoing pitching oscillations near maximum lift.

The response of the full model has been compared to the linear model, where it was seen that the two models give identical results for small amplitude oscillations. For pitching amplitudes above $\Delta\alpha = 2^\circ$ the responses predicted by the full and linearized model are practically identical. The linear state-space formulation of the model is used in the aeroelastic stability tool called HAWCStab [21, 22].

Finally, it is shown that the response of airfoils of finite thickness can be reproduced to a high accuracy by the use of specific inviscid response functions.

References

[1] Petersen, J., "The Aeroelastic Code HawC – Model and Comparisons," *State of the Art of Aeroelastic Codes for Wind Turbine Calculations*, edited by B. M. Pedersen, Vol. Annex XI, International Energy Agency, Technical University of Denmark, Lyngby, April 1996, pp. 129–135.

[2] Petersen, J., Madsen, H., Björck, A., Enevoldsen, P., Øye, S., Ganander, H., and Winkelaar, D., "Prediction of Dynamic Loads and Induced Vibrations in Stall," Tech. Rep. Risø-R-1045(EN), Risø, Roskilde, Denmark, May 1998.

[3] Theodorsen, T., "General Theory of Aerodynamic Instability and The Mechanism of Flutter," *NACA Report 496*, 1935, pp. 413–433.

[4] Fung, Y. C., *An Introduction to the Theory of Aeroelasticity*, John Wiley & Sons, Inc., 1955, (Dover edition, 1993).

[5] Friedmann, P. P., "Formulation and Solution of Rotary-Wing Aeroelastic Stability and Response Problems," *Vertica*, Vol. 7, No. 2, 1983, pp. 101–141.

[6] Tran, C. T. and Petot, D., "Semi-Empirical Model for the Dynamic Stall of Airfoils in View of the Application to the Calculation of Responses of a Helicopter Blade in Forward Flight," *6th European Rotorcraft and Powered Light Aircraft Forum, Papers and Programme*, 1980.

[7] Dat, R. and Tran, C. T., "Investigation of the Stall Flutter of an Airfoil with a Semi-Empirical Model of 2-D Flow," *Vertica*, Vol. 7, No. 2, 1983, pp. 73–86.

[8] Beddoes, T. S., "A Synthesis of Unsteady Aerodynamic Effects Including Stall Hysteresis," *Vertica*, Vol. 1, 1976, pp. 113–123.

[9] Beddoes, T. S., "Representation of Airfoil Behavior," *Vertica*, Vol. 7, No. 2, 1983, pp. 183–197.

[10] Beddoes, T. S., "Practical Computation of Unsteady Lift," *Vertica*, Vol. 8, No. 1, 1984, pp. 55–71.

[11] Leishman, J. G. and Beddoes, T. S., "A Generalized Model for Airfoil Unsteady Aerodynamic Behavior and Dynamic Stall Using the Indicial Method," *Proceedings of the 42nd Annual Forum of the American Helicopter Society*, Washington D.C., June 1986.

[12] Leishman, J. G. and Beddoes, T. S., "A Semi-Empirical Model for Dynamic Stall," *Journal of the American Helicopter Society*, Vol. 34, No. 3, 1989, pp. 3–17.

[13] Leishman, J. G. and Crouse, G. L., "A State-Space Model of Unsteady Aerodynamics in a Compressible Flow for Flutter Analyses," *AIAA Paper 89-0022*, 1989, pp. 1–11.

[14] Leishman, J. G. and Nguyen, K. Q., "State-Space Representation of Unsteady Airfoil Behavior," *AIAA Journal*, Vol. 28, No. 5, May 1990, pp. 836–844.

[15] Leishman, J. G. and Crouse, G. L., "State-Space Model for Unsteady Airfoil Behavior and Dynamic Stall," *AIAA paper 89-1319*, 1989, pp. 1372–1383.

[16] Leishman, J. G., "Two-Dimensional Model for Airfoil Unsteady Drag Below Stall," *Journal of Aircraft*, Vol. 25, No. 7, July 1988, pp. 665–666.

[17] Beddoes, T. S., "A Near Wake Dynamic Model," *American Helicopter Society National Specialists' Meeting on Aerodynamics and Aeroacoustics*, Arlington, February 1987, pp. 1–9.

[18] Leishman, J. G., *Principles of Helicopter Aerodynamics*, Cambridge University Press, 2000.

[19] Van der Wall, B. G. and Leishman, J. G., "On the Influence of Time-Varying Flow Velocity on Unsteady Aerodynamics," *Journal of the American Helicopter Society*, Vol. 39, No. 4, October 1994, pp. 25–36.

[20] Thwaites, B. E., *Incompressible Aerodynamics*, Cambridge University Press, 1961.

[21] Hansen, M. H., "Aeroelastic stability analysis of wind turbines using an eigenvalue approach," *Proceedings of the European Wind Energy Conference*, Madrid, Spain, June 2003, Published on CDrom.

[22] Hansen, M. H., "Aeroelastic eigenvalue analysis of three-bladed wind turbines," *29th European Rotorcraft Forum*, Friedrichshafen, Germany, September 2003, Published on CDrom.

[23] Wagner, H., "Über die Entstehung des dynamischer Auftriebes von Tragflügeln," *Z. angew. Math. u. Mech.*, Vol. 5, 1925, pp. 17–35.

[24] Chow, C. Y. and Huang, M. K., "The Initial Lift and Drag of an Impulsively Started Airfoil of Finite Thickness," *J. Fluid Mech.*, Vol. 118, 1982, pp. 393–409.

[25] Fuglsang, P., "Design and Verification of the RISØ-A1 Airfoil Family for Wind Turbines," *Proc. 39.th Aerospace Sciences Meeting*, Reno, Nevada, USA, January 2001, pp. AIAA 2001–0028.

[26] Jones, R. T., "The Unsteady Lift of a Wing of Finite Aspect Ratio," Tech. Rep. 681, NACA Report, 1940.

[27] Gaunaa, M., *Unsteady Aerodynamic Forces on NACA 0015 Airfoil in Harmonic Translatory Motion*, Ph.D. thesis, Technical University of Denmark, DK-2800 Kgs. Lyngby, Denmark, 2002.

[28] Sørensen, N. N., "General Purpose Flow Solver Applied to Flow Over Hills," Tech. Rep. Risø-R-827(EN), Risø National Laboratory, 1995.

[29] Michelsen, J. A., "Basis3D - a Platform for Development of Multiblock PDE Solvers," Tech. Rep. AFM 92-05, Department of Fluid Mechanics, Technical University of Denmark, 1992.

[30] Michelsen, J. A., "Block-Structured Multigrid Solution of 2D and 3D Elliptic PDE's," Tech. Rep. AFM 94-06, Department of Fluid Mechanics, Technical University of Denmark, 1994.

[31] Abbott, I. A. and Doenhoff, A. E. V., *Theory of Wing Sections*, Dover Publications, 1949.

[32] Øye, S., "Instationære, aerodynamiske kræfter på todimensionalt vingeprofil," Tech. Rep. AFM 81-05, Notat, MEK, Technical University of Denmark, Denmark, November 1981.

[33] Durand, W. F., *Aerodynamic Theory*, Dover, 1943.

A Unsteady flat plate flows

This appendix contains a description of an algorithm for solving unsteady inviscid flat plate flows. According to Glauert [31], it is possible to compute inviscid two-dimensional solutions to the flow over an airfoil of infinitesimal thickness by applying continuous vorticity on the airfoil given by

$$\gamma(\xi,t) = A_0(t)\tan\frac{\Theta}{2} + \sum_{n=1}^{\infty} A_n(t)\sin n\Theta \tag{A.1}$$

$$\xi = \cos\Theta \tag{A.2}$$

Note that ξ is a non-dimensional parameter, describing the position on the chord and in the wake. ξ is zero at mid-chord, minus one and one on the leading edge and trailing edge, as shown in Figure 13. The induced velocity from the bound vorticity on the ξ-axis, which lies on the chordline, is computed from the Biot-Savart law

$$\begin{aligned} v_\eta(\xi,t) &= -\int_{-1}^{1} \frac{\gamma(\xi_1)}{2\pi(\xi-\xi_1)}\,\mathrm{d}\xi_1 \\ &= -1/2A_0(t) - \sum_{n=1}^{\infty} 1/2A_n(t)\cos n\Theta \end{aligned} \tag{A.3}$$

Similarly, the induced velocity from the wake, which is assumed to extend from the airfoil in the chordwise direction, is computed from

$$w_\eta(\xi,t) = \int_{1}^{\infty} \frac{\gamma(\xi_1)}{2\pi(\xi_1-\xi)}\,\mathrm{d}\xi_1 \tag{A.4}$$

The velocity through the airfoil line from the free-stream and the relative motion of the airfoil is

$$u_\eta(\xi,t) = -\dot{y} + (V-\dot{x})\alpha + b(\xi-a)\dot{\alpha} \tag{A.5}$$

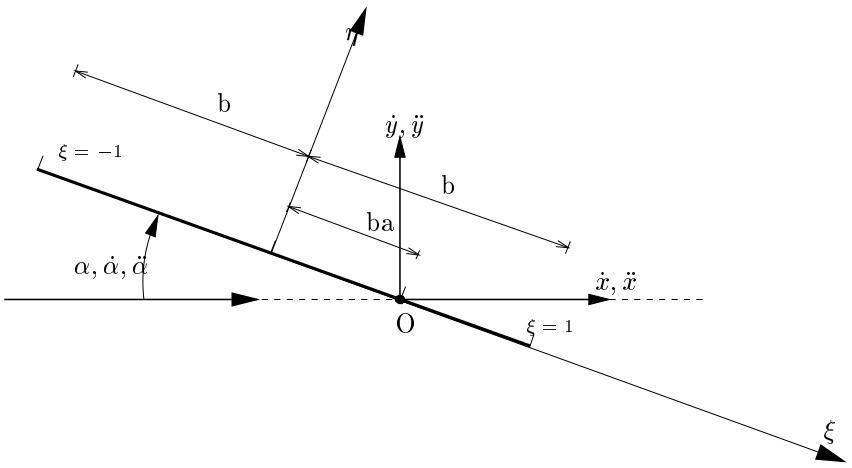

Figure 13. Definitions and positive directions used in the derivations of the general numerical solution. b is the half-chord of the profile, with which the length parameter ξ is normalized. The direction perpendicular to the profile is denoted by η. The angle of attack, α, is determined with respect to the free stream velocity V, and is positive 'nose up'. The translatory motion of the profile is given by x, y, and the derivatives of these, which defines the translatory motion of the hinge-point O, defined by the non dimensional parameter, a, for which the positive direction is towards the trailing edge.

The Neumann boundary condition, stating that the flow through the solid surface be zero, is

$$v_\eta(\xi,t) + w_\eta(\xi,t) + u_\eta(\xi,t) \quad = \quad 0 \tag{A.6}$$

Inserting Equations (A.3)–(A.5) into the Neumann boundary condition, (A.6), yields

$$\begin{aligned} -1/2A_0 - \sum_{n=1}^{\infty} 1/2A_n \cos n\Theta + \int_{-1}^{1} \frac{\gamma(\xi_1)}{2\pi(\xi_1-\xi)}\,\mathrm{d}\xi_1 & \\ -\dot{y} + (V-\dot{x})\alpha + b(\xi-a)\dot{\alpha} \quad &= \quad 0 \end{aligned} \tag{A.7}$$

from which the time dependant coefficients $A_n(t)$ are determined

$$A_0 \quad = \quad 2\{(V-\dot{x})\alpha - \dot{y} - ba\dot{\alpha}\} + \frac{1}{\pi}\int_1^{\infty} \frac{\gamma(\xi)}{\sqrt{\xi^2-1}}\,\mathrm{d}\xi \tag{A.8}$$

$$A_1 \quad = \quad 2b\dot{\alpha} + \frac{2}{\pi}\int_1^{\infty} (\frac{\gamma(\xi)}{\sqrt{\xi^2-1}} - 1)\gamma(\xi)\,\mathrm{d}\xi \tag{A.9}$$

$$A_n \quad = \quad \frac{2}{\pi}\int_1^{\infty} \frac{(\xi-\sqrt{\xi^2-1})^n}{\sqrt{\xi^2-1}}\gamma(\xi)\,\mathrm{d}\xi \tag{A.10}$$

The potential from the bound vorticity on the infinitesimally thick airfoil is

$$\phi(\xi) \quad = \quad \pm 1/2b \int_{-1}^{\xi} \gamma(\xi)\mathrm{d}\xi \tag{A.11}$$

and the jump in chordwise velocity over the airfoil is

$$w_\xi(x) \quad = \quad \pm 1/2\gamma(\xi) \tag{A.12}$$

Plus and minus refers to the upper and lower side of the airfoil, respectively. The total tangential velocity is

$$V_T^2 \quad = \quad (V-\dot{x}+w_\xi)^2 \simeq (V-\dot{x})^2 + 2(V-\dot{x})w_\xi \tag{A.13}$$

Inserting the above in the Bernoulli equation yields for the pressure difference over the airfoil

$$\Delta p \quad = \quad p_l - p_u = \rho(V-\dot{x})\gamma + \rho b\frac{\partial}{\partial t}\int_{-1}^{\xi} \gamma\,\mathrm{d}\xi. \tag{A.14}$$

From this the normal force and moment is integrated

$$N \quad = \quad b\int_{-1}^{1} \Delta p\,\mathrm{d}x = \rho b \int_{-1}^{1} \{(V-\dot{x})\gamma + b\frac{\partial}{\partial t}\int_{-1}^{\xi} \gamma\mathrm{d}\xi\}\,\mathrm{d}\xi \tag{A.15}$$

$$\begin{aligned} M \quad &= \quad b^2 \int_{-1}^{1} (a-\xi)\Delta p\,\mathrm{d}\xi \\ &= \quad \rho b^2 \int_{-1}^{1} (a-\xi)\left((V-\dot{x})\gamma + b\frac{\partial}{\partial t}\int_{-1}^{\xi} \gamma\,\mathrm{d}\xi\right)\,\mathrm{d}\xi \end{aligned} \tag{A.16}$$

Inserting γ from Equation (A.1) and the A_n coefficients from Equations A.8–A.10 yields after considerable reduction [32]

$$\begin{aligned} N &= 2\pi\rho b(V-\dot{x})\left[(V-\dot{x})\alpha-\dot{y}-b(a-0.5)\dot{\alpha}\right] \\ &\quad +\rho b(V-\dot{x})\int_1^\infty \frac{\gamma}{\sqrt{\xi^2-1}}\,\mathrm{d}\xi \\ &\quad +\pi\rho b^2\left[(V-\dot{x})\dot{\alpha}-\ddot{x}\alpha-\ddot{y}-ab\ddot{\alpha}\right] \qquad \text{(A.17)} \\ M &= (a+0.5)b\{2\pi\rho b(V-\dot{x})\left[(V-\dot{x})\alpha-\dot{y}-b(a-0.5)\dot{\alpha}\right] \\ &\quad +\rho b(V-\dot{x})\int_1^\infty \frac{\gamma}{\sqrt{\xi^2-1}}\,\mathrm{d}\xi\}-0.5\pi\rho b^3(V-\dot{x})\dot{\alpha} \\ &\quad +\pi\rho b^3 a\left[(V-\dot{x})\dot{\alpha}-\ddot{x}\alpha-\ddot{y}-ab\ddot{\alpha}\right]-1/8\pi\rho b^4\ddot{\alpha} \qquad \text{(A.18)} \end{aligned}$$

A tangential force arises due to the singularity at the leading edge of the airfoil. This is clearly not physical, but it can be considered the limit of the physical situation when the leading edge radius approaches zero. The tangential force can be expressed as [33]

$$T = -\pi\rho b\left((V-\dot{x})\alpha-\dot{y}-ab\dot{\alpha}+\frac{1}{2\pi}\int_1^\infty \frac{\gamma}{\sqrt{\xi^2-1}}\,\mathrm{d}\xi\right)^2 \qquad \text{(A.19)}$$

The lift and drag coefficients are defined as being perpendicular and parallel to the direction of the free stream velocity, and are determined from a projection of the normal and tangential forces on these directions

$$L = N\cos\alpha - T\sin\alpha \qquad \text{(A.20)}$$

$$D = N\sin\alpha + T\cos\alpha \qquad \text{(A.21)}$$

To determine the wake vorticity, Kelvin's theorem, which states that the total circulation around a closed curve consisting of the same fluid particles is constant, is used. As a consequence of this, the circulation on the profile must be matched by the opposite amount of circulation shed into the flow

$$\Gamma = b\int_{-1}^{1}\gamma\,\mathrm{d}\xi = -b\int_1^\infty \gamma\,\mathrm{d}\xi. \qquad \text{(A.22)}$$

From integration of the bound vorticity, Equation (A.1), we get

$$\Gamma = b\int_{-1}^{1}\gamma\,\mathrm{d}\xi = b\pi(A_0+0.5A_1) \qquad \text{(A.23)}$$

Inserting A_0 and A_1 from Equations (A.8) and (A.9), and using the result from Kelvin's Theorem, Equation (A.22), the following relation is obtained

$$\int_1^\infty \frac{\xi+1}{\sqrt{\xi^2-1}}\gamma\,\mathrm{d}\xi = -2\pi\left[(V-\dot{x})\alpha-\dot{y}-b(a-0.5)\dot{\alpha}\right]. \qquad \text{(A.24)}$$

The above equation can be used to compute the strength of the shed wake vorticity using a numerical approach. The integral in Equation (A.24) can be written as a sum of integrals if the entire wake vorticity from the start of the flow is within the ξ-range covered by the sum

$$\int_1^\infty \frac{\xi+1}{\sqrt{\xi^2-1}}\gamma\,\mathrm{d}\xi = \sum_{i=1}^{N-1}\int_{\xi_i}^{\xi_{i+1}} \frac{\xi+1}{\sqrt{\xi^2-1}}\gamma\,\mathrm{d}\xi \qquad \text{(A.25)}$$

Under the assumption of piecewise constant wake strengths, this can be written as

$$\sum_{i=1}^{N-1}\gamma_i\int_{\xi_i}^{\xi_{i+1}} \frac{\xi+1}{\sqrt{\xi^2-1}}\,\mathrm{d}\xi = \sum_{i=1}^{N-1}\gamma_i\ln\left(\frac{\xi_{i+1}+\sqrt{(}\xi_{i+1}^2-1)}{\xi_i+\sqrt{(}\xi_i^2-1)}\right) \qquad \text{(A.26)}$$

Combining Equations (A.24) and (A.26) it is possible to compute the strength of the newly shed wake

$$\gamma_1 = -\frac{2\pi\left[(V-\dot{x})\alpha - \dot{y} - b(a-0.5)\dot{\alpha}\right] + \sum_{i=2}^{N-1}\gamma_i \ln\left(\frac{\xi_{i+1}+\sqrt{(\xi_{i+1}^2-1)}}{\xi_i+\sqrt{(\xi_i^2-1)}}\right)}{\ln(\xi_2+\sqrt{\xi_2^2-1})}. \tag{A.27}$$

Using Equation (A.27) each time step allows for evaluation of the history of the unsteady wake vorticity, when the dimensionless distances are updated accordingly

$$\overline{\xi}_{i+1} = \left[1 \quad \overline{\xi}_i + \frac{|V_{rel,tail}|\Delta t}{b}\right] \tag{A.28}$$

From the derivation above it is seen that it is possible to determine the forces at any time for any motion of the airfoil by computing the wake strengths using Equations (A.27) and (A.28), and from these compute the forces from the flow using Equations (A.17), (A.18), (A.19), (A.20) and (A.21).

A.1 Verification of the algorithm

To verify that the general numerical solver works as intended, it is compared to analytical and numerical solutions of unsteady incompressible inviscid flat-plate flows. The analytical solutions consist of two well-known solutions, namely an infinitely thin airfoil undergoing impulsive motion, and Theodorsen's solution for oscillating motions of the flat plate for pitching and heaving motions. The response to translatory motion of the flat plate in the free-stream direction is validated using the results from the numerical work of van der Wall and Leishman [19].

Impulsive motion

The response of an impulsively started infinitely thin airfoil was solved by Wagner [23] in 1925. The lift coefficient due to circulation on a strip of unit span as a function of time is

$$C_L = \frac{L}{0.5\cdot\rho c U_0^2} = 2\pi\sin(\alpha)\Phi(\tau), \tag{A.29}$$

where the nondimensional time, τ, is defined as

$$\tau = \frac{2U_0 t}{c}.$$

The exact form of the function, $\Phi(\tau)$, in Equation (A.29) cannot be expressed in analytical terms, but several approximate expressions have been proposed. The most widely used approximate expression, given by R.T. Jones [26] is

$$\Phi(\tau) = 1 - 0.165e^{-0.0455\cdot\tau} - 0.335e^{-0.300\cdot\tau} \tag{A.30}$$

In Figure 14, it is seen that the approximate expression lies very close to (within 1% of) the general flow solution, indicating that the general flow solution obtains correct results.

Oscillating motion

The analytic solution to the forces from an infinitely thin airfoil undergoing harmonic oscillations in angle of attack and heaving motion was first solved analytically by Theodorsen [3] in 1935. Figure 15 show the lift, drag and moment coefficients for the pitching case compared to the results from the present method. It

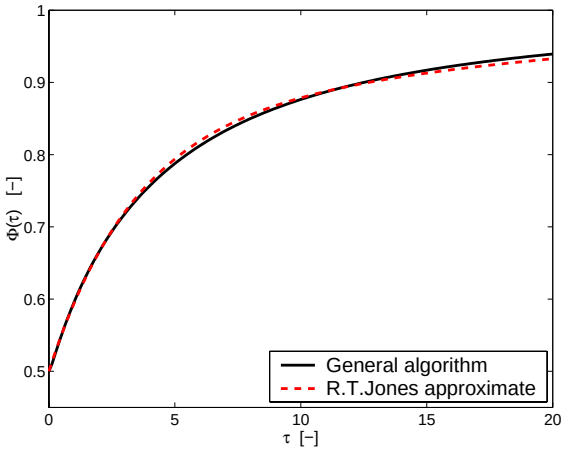

Figure 14. Inviscid response of the lift to a impulsively started flow for a flat plate. Comparison of the approximate expression of Jones [26], Equation (A.30), and the general algorithm.

is seen that the post-transient solution by the general algorithm is in very good agreement with the analytical solution.

To make sure the influence of translatory motion is implemented correctly, Figure 16 show a comparison of the responses of a flat plate to oscillating heaving motion obtained from Theodorsens analytical solution and the present method. As in the previous case, the post-transient agreement is very good.

Since no analytical solution to the problem of a flat plate undergoing harmonic

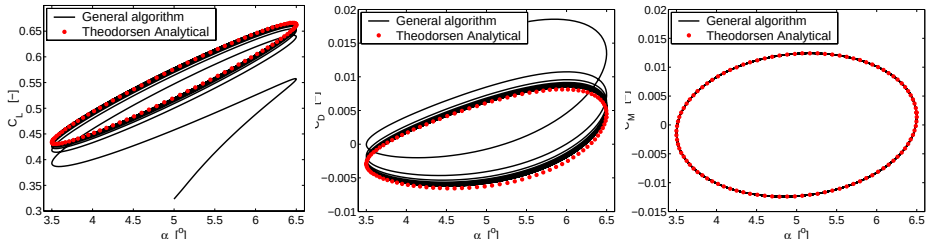

Figure 15. Inviscid response of the lift to oscillating pitching motion for a flat plate; comparison of the analytical expressions by Theodorsen with the general algorithm. Reduced frequency is $k = \omega c/(2U_0) = 0.3$. Angle of attack is $\alpha = 5^\circ \pm 1.5^\circ$, with 1/4 chord as axis of rotation. The left, middle and right graphs show C_L, C_D and C_M, respectively.

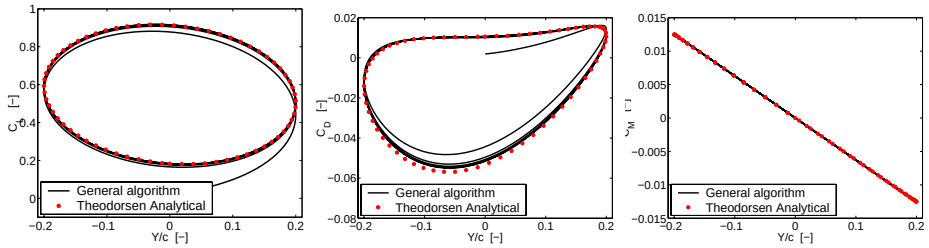

Figure 16. Inviscid response of the lift to oscillating heaving motion for a flat plate; comparison of the analytical expressions by Theodorsen with the general algorithm. The reduced frequency is $k = \omega c/(2U_0) = 0.2$. The left, middle and right graphs show C_L, C_D and C_M, respectively.

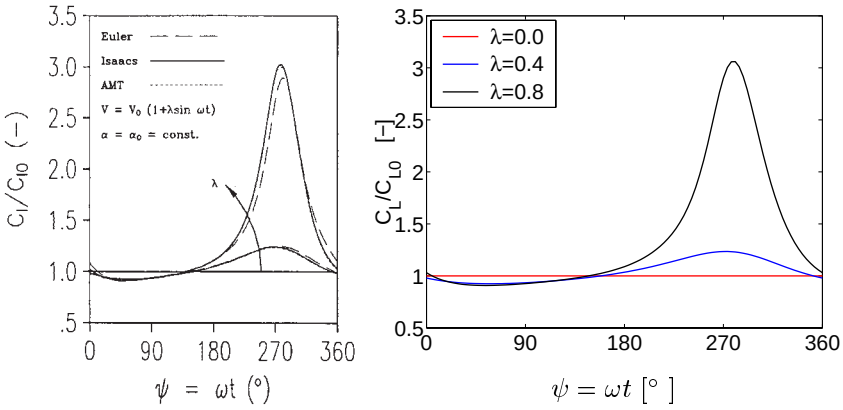

Figure 17. Inviscid response of the lift to oscillating motion in the streamwise direction for a flat plate; comparison of the numerical work of van der Wall and Leishmann [19] (left graph, reproduced from [19]) with the general algorithm (right graph). The reduced frequency is $k = \omega c/(2U_0) = 0.2$, and the harmonic motion in the streamwise direction corresponds to maximum translatory velocity $V\lambda$.

translatory motion in the direction of the free-stream is known to the authors, a comparison with the numerical work of van der Wall and Leishmann [19] is shown in Figure 17.

It is observed that the results of the present algorithm agrees very well with the results of van der Wall and Leishman, thereby concluding the successful verification of the general numerical solution methodology to unsteady inviscid flat plate flows proposed here.

Bibliographic Data Sheet **Risø–R–1354(EN)**

Title and author(s)

A Beddoes-Leishman type dynamic stall model in state-space and indicial formulations

Morten Hartvig Hansen, Mac Gaunaa, Helge Aagaard Madsen

ISBN	ISSN
87-550-3089-0; 87-550-3090-4 (Internet)	0106–2840

Dept. or group	Date
Aeroelastic Design Wind Energy Department	June 18, 2004

Groups own reg. number(s)	Project/contract No.
	ENS 1363/00-0007 ENK6-CT2000-00320

Pages	Tables	Illustrations	References
40	1	17	33

Abstract (Max. 2000 char.)

This report contains a description of a Beddoes-Leishman type dynamic stall model in both a state-space and an indicial function formulation. The model predicts the unsteady aerodynamic forces and moment on an airfoil section undergoing arbitrary motion in heave, lead-lag, and pitch. The model includes the effects of shed vorticity from the trailing edge (Theodorsen Theory), and the effects of an instationary trailing edge separation point. The governing equations of the model are nonlinear, and they are linearized about a steady state for application in stability analyzes. A validation is carried out by comparing the response of the model with inviscid solutions and observing the general behavior of the model using known airfoil data as input. The proposed dynamic model gives results identical to inviscid solutions within the attached-flow region; and it exhibits the expected dynamic features, such as overshoot of the lift, in the stall region. The linearized model is shown to give identical results to the full model for small amplitude oscillations. Furthermore, it is shown that the response of finite thichkness airfoils can be reproduced to a high accuracy by the use of specific inviscid response functions.

Descriptors INIS/EDB

WIND TURBINES; AERODYNAMICS; AEROELASTICITY; DYNAMICS